Textile Research Journal

http://trj.sagepub.com

Mechanical Properties of Fabric Woven from Yarns Produced by Different Spinning Technologies: Yarn Failure in Woven Fabric

Moon H. Seo, Mary Lynn Realff, Ning Pan, Mary Boyce, Peter Schwartz and Stanley Backer

Textile Research Journal 1993; 63; 123
DOI: 10.1177/004051759306300301

The online version of this article can be found at:
http://trj.sagepub.com/cgi/content/abstract/63/3/123

Published by:
SAGE Publications
http://www.sagepublications.com

Mechanical Properties of Fabric Woven from Yarns Produced by Different Spinning Technologies: Yarn Failure in Woven Fabric[1]

MOON H. SEO,[2] MARY LYNN REALFF,[3] NING PAN,[4] MARY BOYCE, PETER SCHWARTZ,[5] AND STANLEY BACKER

Department of Mechanical Engineering, Massachusetts Institute of Technology, Cambridge, Massachusetts 02139, U.S.A.

ABSTRACT

A study has been conducted on the mechanisms of in-situ tensile failure of staple yarns during uniaxial tensioning, as in a conventional ravel strip test. The yarns were PET/cotton blends processed on ring, rotor, and airjet spinning systems, and then woven into plain or twill weave fabrics. Load-extension behaviors of the yarns were recorded for the in-fabric state as well as for the free state (out-of-fabric), and SEM comparisons were made of the fractured yarn ends obtained in the two states. When the tensioned yarns became jammed between cross yarns before straightening, the fracture ends were abrupt, similar to those observed in near zero gauge length tests of free-state yarns. However, when fabric structure was such that tensioned yarns could straighten without cross yarn jamming, the resulting failure zones were considerably longer, with a mixture of fiber fracture and slippage similar to that observed in long gauge length tests of free-state yarns. The interaction between yarn properties and weave geometry had a strong influence on the local disturbance of cloth structure resulting from isolated yarn failure during fabric tensioning. The extent of such disturbance permitted estimates of the stress recovery length of the failed yarn and showed its dependence on cloth tightness and yarn type.

In many cases, a woven fabric exhibits a much higher strength than that predicted from the strengths of its constituent yarns tested at the same gauge length [5, 6, 12]. Such discrepancies have been termed *fabric assistance.* Lord and Radhakrishnaiah [5, 6] discussed fabric assistance for different yarn systems, showing relatively higher assistance for friction and rotor spun yarns than for ring spun yarns of comparable size. They associated this with contact pressures at yarn crossovers, explaining that yarns in denser fabrics experience closer contact pressure zones along their length, and so there is less chance for in-fabric yarn failure than in less dense fabrics.

In providing further explanations of such fabric assistance, Shahpurwala and Schwartz [12] have defined the term "overload" or "subbundle" length to represent a short segment of yarn possessing the appropriate mean strength and strength distribution to permit valid prediction of fabric strength. In practice, they first determined the mean strength and strength distribution of yarns removed from the fabric and tested at a 152.4 mm gauge length. Then, using weakest link theory with equal load sharing and with local load sharing rules, they scaled down to the appropriate subbundle length to match fabric strength, also measured at a 152.4 mm gauge length. Then they used the subbundle length in a statistical model of fabric strength in a manner analogous to that employed in composite materials models. The subbundle lengths for the cotton yarn fabrics in equal-load and local-load sharing cases were thus estimated to be less than 17 mm, shorter than the average cotton staple length of the yarn used in the test fabrics.

These quantities, it should be noted, were based solely on statistical considerations, *i.e.*, weakest link theory, not micromechanical analysis. Shahpurwala and Schwartz [12] further illustrated fabric assistance by defining a *friction factor,* which combined yarn size,

[1] This paper was presented at the December 10, 1991 Technical Conference of The Fiber Society in New Orleans, LA.

[2] Present address: Konkuk University, Seoul, Korea.

[3] Present address: Georgia Institute of Technology, Atlanta, GA.

[4] Present address: University of California, Davis, CA.

[5] Present address: Cornell University, Ithaca, NY.

relative number of yarn interlacings (with respect to that of plain weave), and crimp ratio of yarns in loading and cross directions. This friction factor had a positive correlation with the observed differences between yarn-based predictions of fabric strength and actual fabric test results.

If a chain-of-bundles model is to be applied to yarn failure in a fabric, there must be enough shear force between yarn segments of subbundle length and the cloth matrix to satisfy independence of yarn failure in each subbundle. If this condition is met, then fabric tensile strength will reflect yarn tensile behavior at subbundle lengths.

In an earlier paper [10], we showed, through a statistical analysis of tensile tests and scanning electron microscope (SEM) observations, that the tensile failure mechanism of individual staple yarns in short gauge lengths (<25.4 mm) is mechanistically different from that at long gauge lengths (>76.2 mm). This difference can be primarily explained by considering the increased relative number of fibers that are held by both grips as the test gauge length decreases. The question remains as to how yarn gripping occurs within a tensioned woven fabric.

The objective of this paper is to compare the tensile stress-strain behavior of constituent yarns *in a fabric* and *out of a fabric*, and to identify the dominant yarn failure mechanisms in each of these test conditions for different woven fabric geometries.

Experiments

Two sets of fabrics were tested. The first set, a G series, consisted of ring spun and rotor spun PET/cotton yarns in a 2/1 twill weave. In this paper, we refer to these yarns as ring G and rotor G. The second set, an S series, consisted of ring spun and airjet spun yarns, in a plain weave. Here, they will be referred to as ring S and airjet S yarns. These yarns and fabrics are described in Tables I and II.

For the tensile tests of constituent yarns out of fabrics, yarns were removed from the fabrics and stored under standard testing conditions (20°C and 65% RH) for 24 hours before testing. Tensile tests of these yarns were run at two different gauge lengths following different procedures. In one case (procedure I), the yarn specimen lengths, 12.7 mm and 127 mm, were measured under a low preload (5 g) and then tested with 12.7 mm and 127 mm initial grip separation. In the other case (procedure II), the yarn specimens were taken from 127 mm fabric specimens and tested at 127 mm initial grip separation; therefore, the actual yarn specimen length in the latter case was longer than in the former case, despite the use of the same initial grip separation distance, 127 mm. The tensile test was conducted at a strain rate of 0.1 min^{-1} with respect to initial grip separation distance on an Instron tensile tester.

The fabric tensile test was conducted using a 127 mm by 25.4 mm wide ravel strip geometry with a strain rate of 0.1 min^{-1}. The tensile failure process was monitored using a digital oscilloscope and video camera in order to identify isolated yarn breaks in the fabric. In most cases, several initial isolated breaks were positively identified by observing load drop, as well as visual observation of the actual local yarn failure. However, the several isolated breaks that occurred at the instant of

TABLE I. Series G 2/1 twill fabrics and their yarns.

	Ring G		Rotor G	
Spin system	Warp	Fill	Warp	Fill
Yarn size, C.C.	15.5	12.0	15.5	12.0
Twist mult.	4.2	4.2	3.7	3.7
Composition	PET/cotton	PET/cotton	PET/cotton	PET/cotton
Percentages	50/50	50/50	50/50	50/50
Fabric count, yarns/25.4 mm	88	50	86	50

TABLE II. Series S plain weave fabrics and their yarns.

	Ring S		Airjet S	
Spin system	Warp	Fill	Warp	Fill
Yarn size, C.C.	26	26	26	26
Twist mult.	3.91	3.91	–	–
Composition	PET/cotton	PET/cotton	PET/cotton	PET/cotton
Percentages	65/35	65/35	65/35	65/35
Fabric count, yarns/25.4 mm	102	54	102	54

final failure could not be individually identified by the load signal response.

The tensile tested yarn ends *in* and *out* of fabric were then observed under the optical microscope and the scanning electron microscope (Cambridge, S204) at 1.5 kV accelerating voltage, after gold coating.

For fabric casting in the strained state, loaded (strained) fabrics were clamped in a separate frame, then cast with transparent unsaturated PET styrene resin (Castolite). Strain frozen fabric cross sections were then observed under the optical microscope and their yarn paths were traced as illustrated in reference 3, p. 52. The lateral force and contact pressure on the tensioned yarns were then estimated.

Comparisons of Stress-Strain Curves of Fabrics and of Their Constituent Yarns

In the earlier paper [10], we demonstrated that in tensile tests of staple yarns, there are differences in yarn failure mechanisms between specimens tested at gauge lengths longer or shorter than the staple length.

Figures 1 and 2 show the typical *out-of-fabric* stress-strain diagrams for 12.7 mm and 127 mm gauge lengths of PET/cotton warp and filling yarns taken from the G-series fabrics. For both yarn systems, the results show larger breaking strains for the shorter gauge length than for the longer gauge length. The local yarn slippage in the (constant pressure Instron) grips, is primarily a function of tensile load during the test, regardless of gauge length involved. In long specimens, such jaw slippage may be neglected; in short gauge tests (such as 12.7 mm), jaw slippage is of the same order as the specimen displacement reading and hence distorts the strain values. The 127 mm data in Figure 1 show lower breaking strain for the rotor spun yarn versus the ring spun yarn. Generally the results were similar for the 12.7 mm gauge length tests, so far as rankings of breaking strains were concerned, although the absolute strain value of the short gauge tests, we repeat, were significantly affected by jaw slippage. The purpose of reporting the short gauge data here is only to depict the overall shapes of the stress-strain curve and, in particular, its peak values.

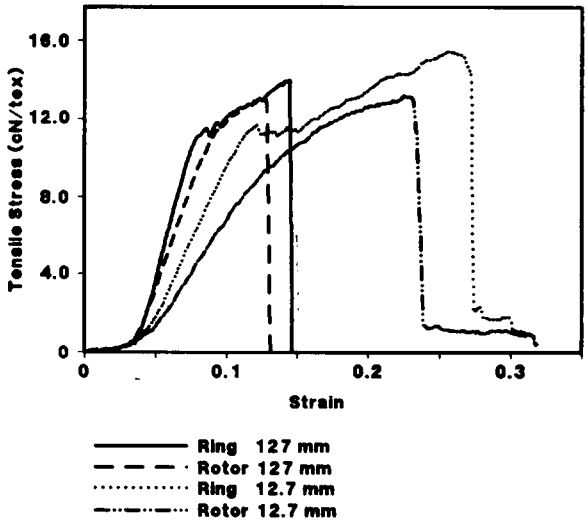

FIGURE 1. Stress-strain curves at 127 and 12.7 mm gauge lengths of the ring G and rotor G warp yarns tested out of fabric at 0.1 min^{-1} strain rate (Procedure I).

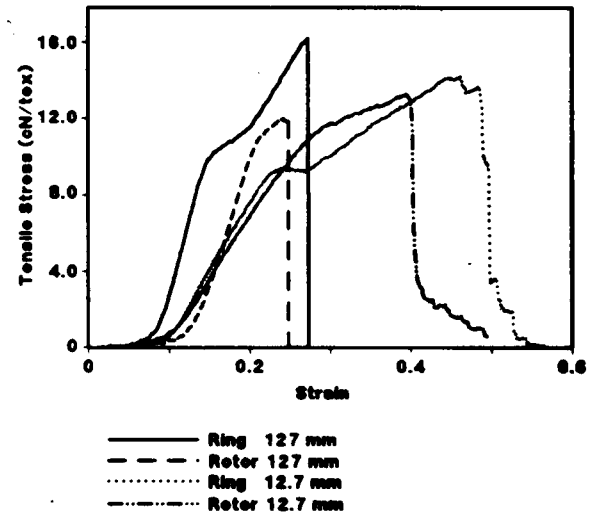

FIGURE 2. Stress-strain curves at 127 and 12.7 mm gauge lengths of the ring G and rotor G filling yarns tested out of fabric at 0.1 min^{-1} strain rate (Procedure I).

For the G-series yarns, the general shape of the stress-strain curves differs somewhat between the ring and rotor spun yarns, although their nominal count is the same. The stress-strain curves of the ring spun yarns at 127 mm gauge length can be divided into at least three regimes (Figures 1 and 2): an initial, nonlinear regime, a secondary, linear regime, and a third, low average tangential modulus regime with load undulations. From studies of blended twisted yarns [7, 8] and staple yarns at small extensions [2, 9], we know that the two initial zones reflect the cooperative contribution of the cotton and PET fiber stress-strain behavior; the third regime reflects the stress-strain behavior of the PET fibers accompanied by multiple breakage of cotton fibers. Therefore, the boundary between the second and third regimes should be yarn strain, which can initiate cotton fiber breakage in a blended yarn.

Figure 3 depicts typical fabric stress-strain curves of the ring G and the rotor G series for warp direction loading. These curves have been normalized with respect to the number of yarns loaded in the 25.4 mm ravel strip width. The stress-strain curves of the G fabric pair show a shape similar to those of the constituent yarns tested out of fabric at the 127 mm gauge length (Figure 1).

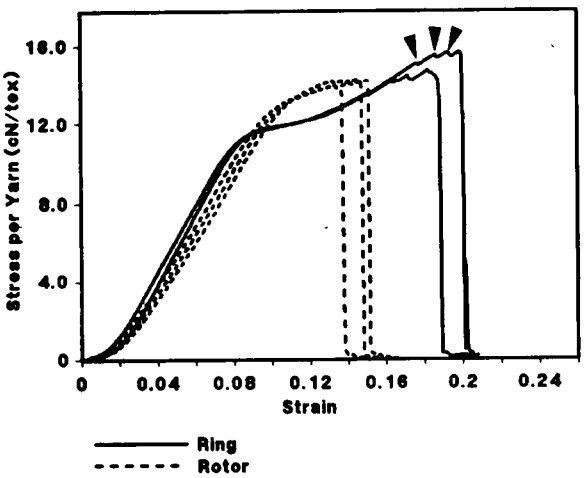

FIGURE 3. Warp direction stress-strain curves of ring G and rotor G fabrics at 127 mm gauge lengths at 0.1 min^{-1} strain rate.

Fabric Failure Process and Isolated Yarn Failure

When testing the G fabric set in both the warp and filling directions, the final catastrophic failure in the ravel strip test was preceded by several isolated yarn failures. In a separate set of experiments involving the S series fabrics, the isolated breaks occurred only in filling direction tests. Whenever there was an isolated yarn failure, we identified a corresponding tensile load drop, as marked with arrows in Figure 3, and visual observation after failure with the aid of video camera recording.

Figures 4a–d are photographs of isolated yarn breakage in the G fabrics, which occurred during uniaxial tensile testing. The presence of isolated breaks is revealed by horizontal light streaks in the dark fabric surfaces. The fabrics in question had been piece dyed, and the local displacement of the isolated broken yarn or yarns exposed the relatively undyed contact zone between warp and filling. We also tested an additional set of ring S and airjet S fabrics and examined them for isolated breaks in much the same manner as above. Both S and G fabrics exhibited more isolated yarn breakage in filling directional loading than in warp directional loading. Ring G fabric experienced more isolated breaks than rotor G fabric. Ring S fabric experienced more isolated breaks than airjet S fabrics. The differences applied in both directions of loading. General rankings can be made for the number of isolated breaks observed:

(a) Ring G fill > rotor G fill > ring G warp > rotor G warp.

(b) Ring S fill > airjet S fill > ring S warp > airjet S warp.

The final catastrophic fabric failures occurred in a region where there were multiple isolated failures. The number of clearly identifiable isolated yarn breaks that remained in the broken fabric segments were not more than two for all cases examined. When multiple isolated yarn breaks occurred, there were isolated breaks in adjacent yarns, in many cases, separated by one or more unbroken yarns.

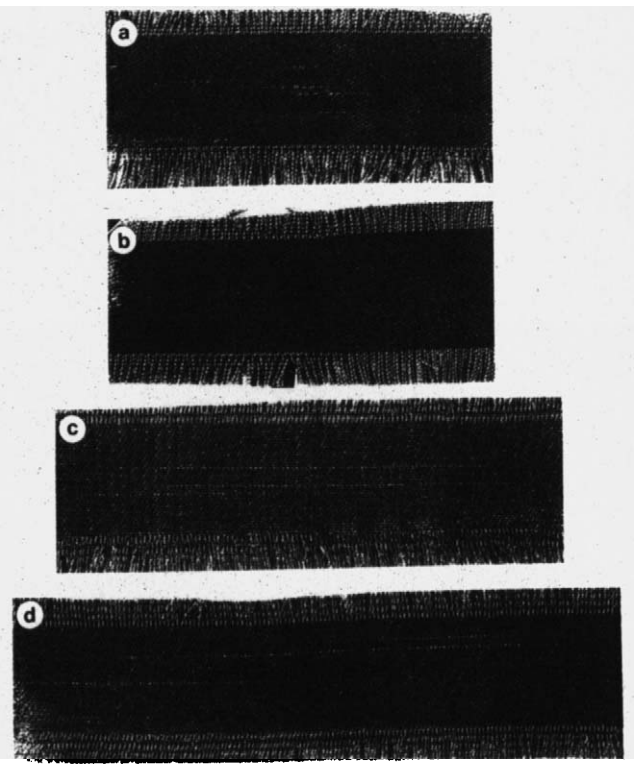

FIGURE 4. View of isolated failures in the ring G (a) and rotor G (b) fabric tested in warp direction at 127 mm gauge length, and of isolated failures in the ring G (c) and rotor G (d) fabric tested in the filling direction at 127 mm gauge length.

There was no direct physical evidence establishing the cause of isolated failure at any specific points in the fabrics tested. One would expect that the weakest location would result in the first isolated breakage point. The next failure should then occur at the next weakest yarn location with respect to specific yarn load at that instant, including any overload from an earlier adjacent isolated break. This process would then continue until the final, critical size of multiple adjacent breaks could be reached.

In general, a single isolated yarn failure in test fabrics displayed the following process: First, a slight tensile load drop occurred during the displacement driven tensile test. Then, longitudinal retraction of both failed yarn ends took place, resulting in separation of the fractured ends and distortion of the local cross yarns, which were frictionally resisting this retraction. The distance between the broken yarn ends and the point where the yarn resumed its undisturbed position and its fully recovered tension in the fabric was termed its recovery length. In addition, the crowns of failed ends protruded from the plane of the fabric.

Two characteristic fracture modes occurred in yarns that had failed in isolated instances during tensioning of the fabrics. One mode was very abrupt with virtually all fibers fractured across the yarn section within a narrow zone. Figure 5a illustrates the abrupt yarn break that occurred in a ring spun fabric tested in the warp direction of a 127 mm gauge fabric specimen. The yarn in Figure 5a was taken from a twill fabric. Figure 5b shows an isolated rotor yarn break taken from a warpwise tensioned twill fabric. Finally, Figure 5c shows the abrupt failure that occurred in an airjet yarn when tested fillingwise in a 127 mm plain weave specimen.

Clearly all of these samples showed strikingly abrupt yarn breaks with very short fiber tails. For both PET and cotton, the fiber ends exhibited tensile failure characteristics. None of these fiber tails exceeded one fabric repeat unit in length and, as a whole, the yarn ends had a shape similar to that observed in out-of-fabric yarn tests at near zero gauge length [10]. Such abrupt yarn failure was indicative of fiber fracture propagation across a narrow zone, and reflected extremely local load sharing of constituent fibers facilitated by high lateral pressures.

In most cases, failure occurred at a point where the yarn was in a bent configuration, giving evidence of the effect of lateral pressure afforded by fabric structure. More evidence of high lateral pressure in the ring G fabric is provided in Figure 6, which shows highly deformed fiber ends of a ring spun yarn that failed in a warpwise test of a 127 mm fabric specimen.

Figure 7 shows a most interesting failure pattern along the length of a yarn that had experienced an isolated break. At several points removed from the abrupt yarn failure zone, regions of broken fibers can

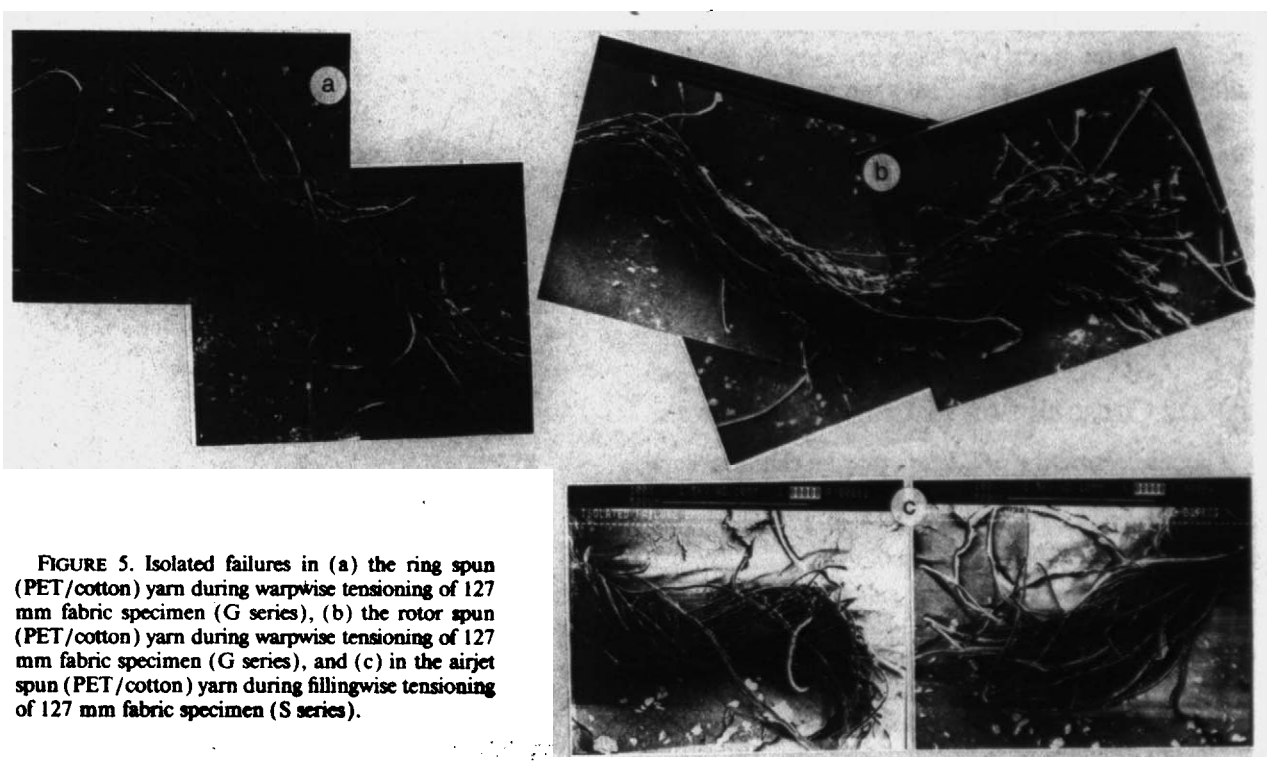

FIGURE 5. Isolated failures in (a) the ring spun (PET/cotton) yarn during warpwise tensioning of 127 mm fabric specimen (G series), (b) the rotor spun (PET/cotton) yarn during warpwise tensioning of 127 mm fabric specimen (G series), and (c) in the airjet spun (PET/cotton) yarn during fillingwise tensioning of 127 mm fabric specimen (S series).

FIGURE 6. Deformed fiber end in isolated ring spun yarn fracture during warpwise tensioning of 127 mm woven fabric specimen (G series).

be seen (as designated by arrows). The fabric from which the yarn of Figure 7 was withdrawn was a 2/1 twill. Here, localized fiber failure occurs in the *inside* of the yarn bend, contrary to expectation of simple theory. Because of yarn crimping due to weave structure, the yarn may be viewed as a pre-bent curved beam rather than an ordinary beam. After the fabric is produced and fully relaxed, the fibers tend to be in a stress-free state. Therefore, upon tensile loading of the fabric, it follows that, due to *unbending,* the inside of the yarn suffers the maximum tensile stress.

In contrast to Figures 5a–c, Figures 8a–b show ring and rotor spun yarns that have experienced isolated failure in a 127 mm specimen when tested in the fillingwise direction. These yarn breaks are drastically different from the set contained in Figures 5a–c and Figure 7, and reflect a combined fiber fracture/slippage mode of failure rather than a local rupture propagation. They were more characteristic of yarn failure patterns obtained in long gauge length tests of yarns tested out of the fabric [10].

Fabric Constraint on its Constituent Yarns

The microstructure of a fabric may be characterized by two orthogonal sets of yarns that periodically undulate with respect to one another. For convenience in discussing uniaxial loading of fabrics, yarns parallel to the loading direction will be called "loaded" yarns and the orthogonal yarns "cross" yarns. Uniaxial tensile loading of a fabric introduces normal forces between the loaded yarn and the cross yarn. As a result of this, the local curvature of the loaded yarn decreases and the local curvature of the cross yarn increases; this is

FIGURE 7. Multiple local fiber breakage along a ring spun warp yarn after isolated failure (G series). Arrows indicate multiple fiber breaks.

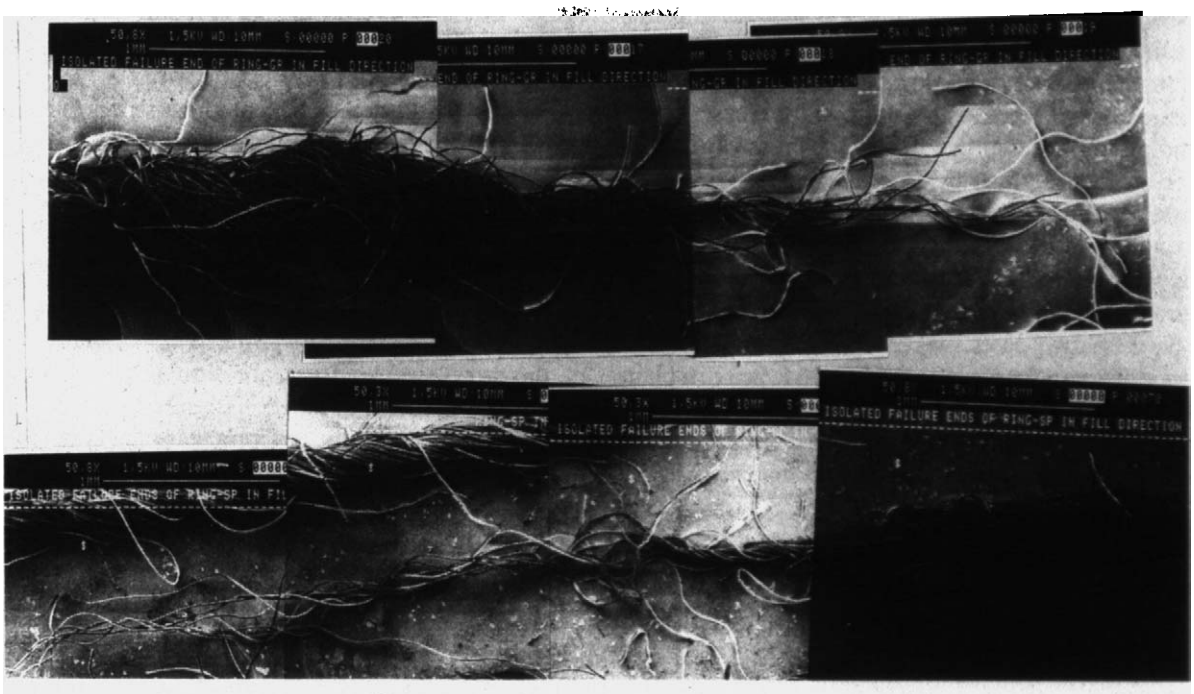

FIGURE 8. Isolated failures in the ring spun (PET/cotton) yarn during fillingwise tensioning of 127 mm fabric specimen: (top) G series, (bottom) S series.

the well documented phenomena of *crimp interchange* [3].

In order to examine fabric constraint effects on yarn response, it is instructive to compare stress-strain curves of a load bearing yarn within a fabric to that of a constituent yarn out of the fabric. Figure 9 shows schematics of the constituent yarn deformation process in the plain weave fabric structures during uniaxial tensioning. When a fabric specimen is strained, the yarn in the fabric will be strained in its inclined state due to the presence of the cross yarn. However, the yarn removed from the fabric and tensile tested will not ex-

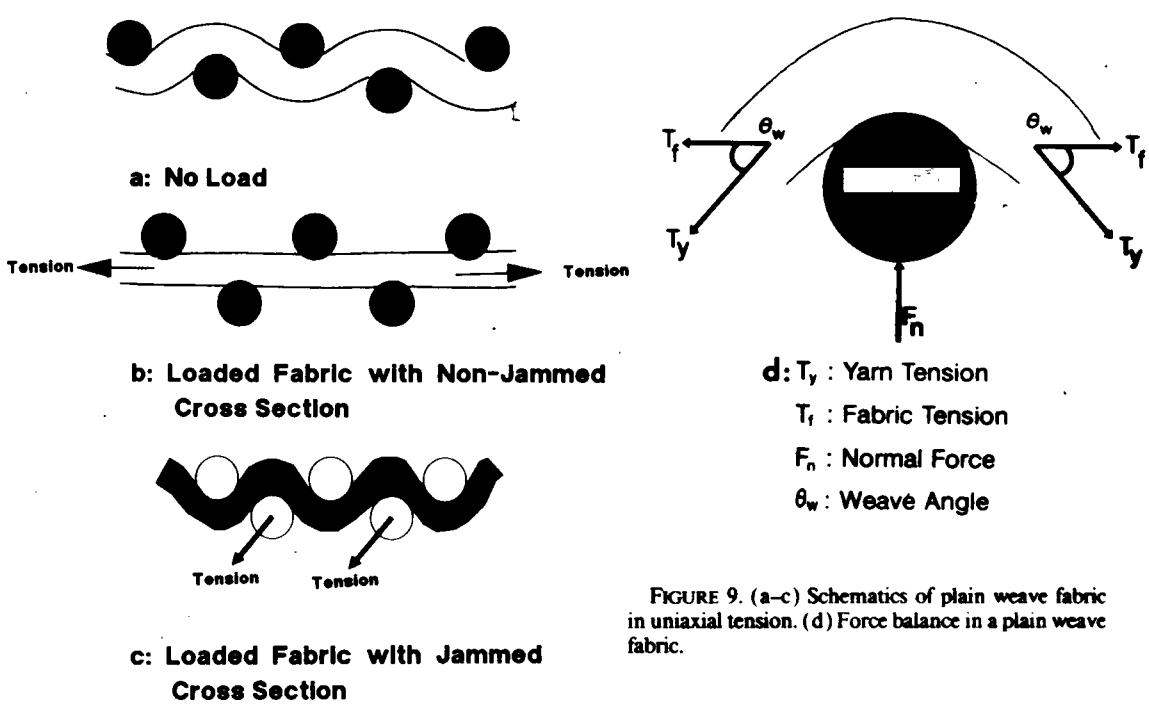

FIGURE 9. (a–c) Schematics of plain weave fabric in uniaxial tension. (d) Force balance in a plain weave fabric.

perience appreciable load until the extra crimp disappears. When there is sufficient cross yarn length per unit structure, the loaded yarn becomes *nearly* straight, and the normal force acting on it will increase, corresponding to increased bending of the cross yarn as depicted in Figure 9b. If there is insufficient cross yarn length per unit cell of the weave, however, the cross yarn will jam and extend somewhat, but the loaded yarn will remain bent at the contact zone as shown in Figure 9c.

For these two cases, we can make a simple force balance diagram for a segment of loaded yarn in a plain weave fabric as depicted in Figure 9d [11]. If no shear force interaction is assumed between adjacent loaded yarns, the yarn tension T_y can be estimated as

$$T_y = \frac{T_f}{\cos \theta_w} \quad , \tag{1}$$

where T_f = fabric tension per each load bearing yarn, T_y = yarn tension, and θ_w = weave angle.

When the yarn stress-strain curve is assumed to be linear, the stress-strain curve at any load can be expressed as

$$T_f = E_y \epsilon_y \cos \theta_w \tag{2}$$

$$= E_f \epsilon_f \quad , \tag{3}$$

where E_y = yarn modulus, ϵ_y = yarn strain, and ϵ_f = fabric strain.

For simplicity, the fabric thickness is assumed to be constant with small weave angle changes; the strain relationship between yarn and fabric can be approximated as

$$\epsilon_y = \epsilon_f \cos^2 (\theta_w) \quad , \tag{4}$$

and the ratio of fabric modulus to yarn modulus depends on the third power of the cosine of the weave angle:

$$\frac{E_f}{E_y} = \cos^3 (\theta_w) \quad . \tag{5}$$

The normal force F_n at the contact zone can be approximated as

$$F_n = 2T_y \sin (\theta_w) \quad . \tag{6}$$

Combining Equations 5 and 6, we can show that

$$\left(\frac{E_f}{E_y}\right)^{2/3} + \left(\frac{F_n}{2T_y}\right)^2 = 1 \quad , \tag{7}$$

which indicates that the ratio between the fabric modulus E_f and the yarn modulus E_y can be used as not only a measure of predicting yarn geometry in a loaded fabric, but also as a rough measure of normal force between warp and filling yarns for a given "loaded" fabric constructed of linear elastic yarns.

Figures 10a–d depict typical stress-strain curves of the G and the S fabric series, tested in the warp and the filling directions, and curves of their constituent yarns. The fabric curves have been normalized with respect to the number of yarns loaded in the ravel strip test. The initial parts of the stress-strain curves for all these constituent yarns show a near zero tensile load due to excessive length and crimp. The remaining parts of the stress-strain curves are similar to the results shown in Figures 1, 2, and 3. Though the stress-strain curves of yarns from the different spinning systems are not linear in all strain ranges, a significant portion of a linear regime (regime 2) can be found. Table III shows the fabric-to-yarn modulus ratio of such linear regimes, which were measured near 30% of the yarn breaking stress. It also includes the calculated normal force ratios based on Equation 7. All of these values were measured from Figures 10a–d.

The results above show that except for the airjet yarn fabric, all other *warp* direction fabric test results manifested significantly lower modulus ratio values than tests in the *filling* direction. Also, except for the airjet yarn fabric, the estimated normal force ratios were much higher in the warp direction than in the filling direction. However, with regard to normal force ratios, the air jet fabrics exhibited significantly higher normal force ratios in the filling direction than in the warp direction. A high normal force ratio implies the presence of high fabric constraint, while a low normal force ratio indicates minimal constraint. This is illustrated in the fillingwise rupture photographs of the airjet spun fabric (Figure 5c), which highlight local fiber failure with negligible slippage, a condition typical of high fiber constraint. The ring and rotor fabrics (Table III) have much lower normal force ratios in the filling direction, thus reflecting lower fabric constraint on the filling yarns. As a result, rupture of the filling yarns in these fabrics consists of combined fiber rupture and considerable slippage, as shown in Figures 8a and b.

We attempted a direct measurement of fabric constraint relative to its constituent yarns by observing strained fabric cross sections. Figures 11a–d depict the trace line of a loaded yarn and a cross yarn in a fabric tensioned to 30% of its breaking stress in the *warp* direction. Jamming of the filling yarn occurred at 30% of the fabric breaking strength during warp-wise loading (Figures 11b and d), while the longitudinal section along the loaded warp yarn showed reduced undulation amplitude (Figures 11a and c), which indicates crimp

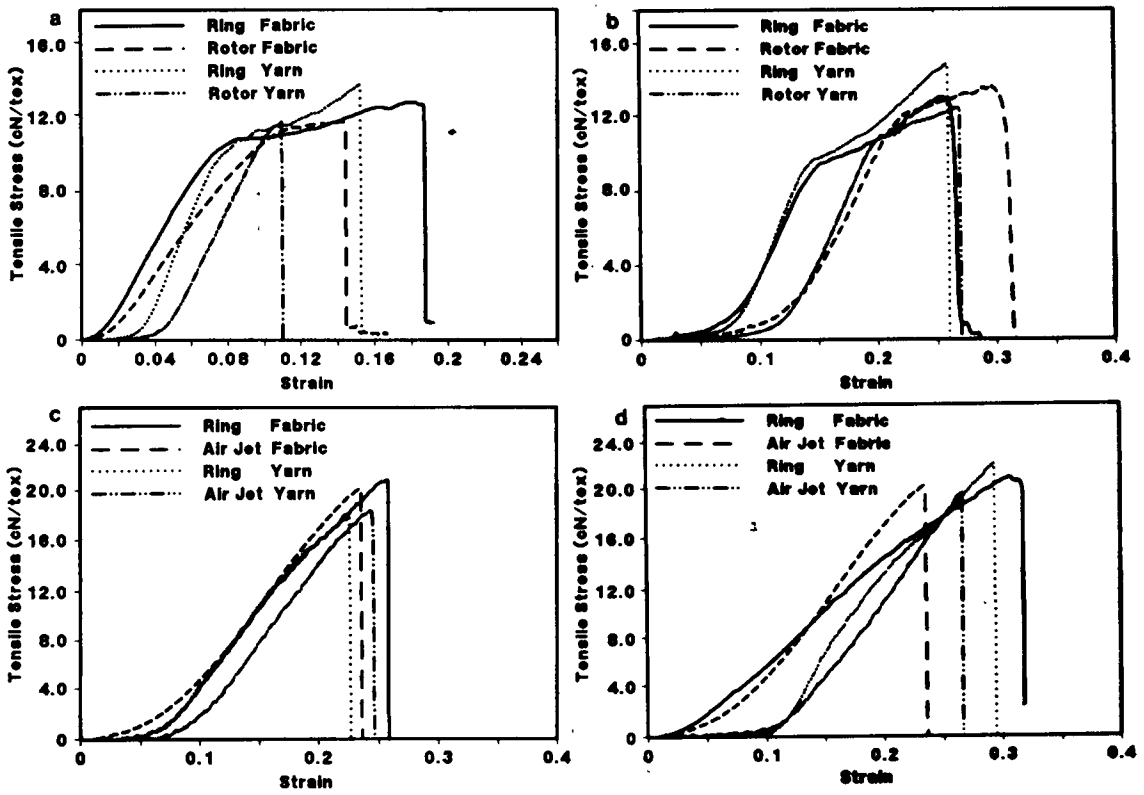

FIGURE 10. Stress-strain curves of the ring G and rotor G fabrics in (a) the *warp direction* and their constituent *warp yarns* tested at 127 mm gauge length at 0.1 min^{-1} strain rate, and (b) the *filling direction* and their constituent *filling yarns* tested at 127 mm gauge length at 0.1 min^{-1} strain rate. (c) Stress-strain curves of the ring S and airjet S fabrics in the *warp direction* and their constituent *warp yarns* tested at 127 mm gauge length at 0.1 min^{-1} strain rate, and (d) the *filling direction* and their constituent *filling yarns* tested at 127 mm gauge length at 0.1 min^{-1} strain rate.

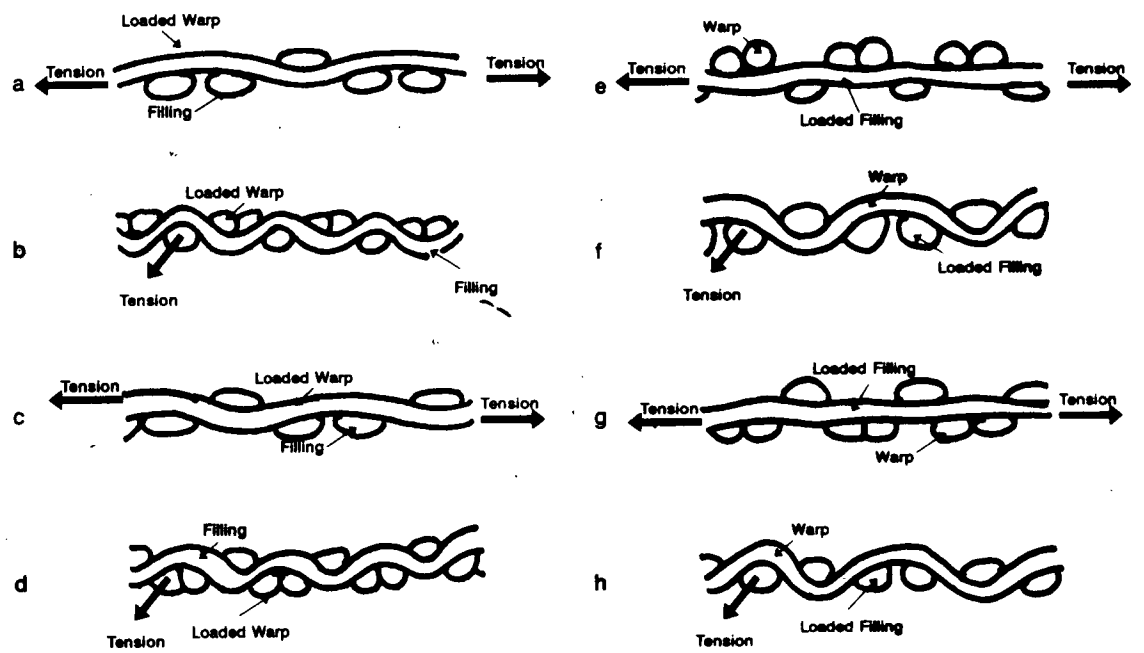

FIGURE 11. Trace of yarns in ring (a, b) and rotor spun (c, d) 2/1 twill fabric (G series) loaded warpwise to 30% of breaking strength, ring (e, f) and rotor spun (g, h) 2/1 twill fabric (G series) loaded fillingwise to 30% of breaking strength.

TABLE III. Modulus ratios and normal force ratios between fabrics and their constituent yarns.

	Modulus ratio, $\frac{E_F}{E_y}$	Normal force ratio, $\frac{F_n}{T_y}$
Ring G		
warp	0.73	0.87
fill	0.84	0.66
Rotor G		
warp	0.68	0.95
fill	0.94	0.40
Ring S		
warp	0.47	1.25
fill	0.99	0.16
Airjet S		
warp	0.93	0.43
fill	0.81	0.72

interchange. Since the filling cross yarn was jammed at 30% loading of the warp yarns, little structural change could be expected thereafter. The loaded warp yarns remained bent until failure, and thus normal forces at yarn contact points were high. As a result, fabric constraint on the loaded yarn was relatively high.

In a fiber-reinforced composite material, increased lateral pressure can reduce local critical lengths and produce greater efficiency in load transfer from the matrix to the fiber. In a yarn structure, a decrease in the critical length in effect increases the constituent fiber strength efficiency, thereby increasing the apparent strength of the yarn [13, 14, 15]. However, the local high normal pressure may also deform the fiber geometry in the contact zone and could thus reduce the fiber strength [4].

In contrast to Figures 11a–d, Figures 11e–h display the cross sections of fabrics tensioned in the *filling* direction at 30% of the breaking stress. In this case, there was no jamming of the warp yarn. Since the loaded filling yarn was essentially straight for both ring and rotor yarns (Figures 11e and g), we expected little difference between yarn and fabric stress-strain curves. Hence, the fabric-to-yarn modulus ratio was high (as shown in Table III). Fabric constraint on these straight filling yarns was accordingly minimal, thus leading to combined fiber rupture/slippage (Figures 8a and b).

Analysis of Yarn Failure Mechanism in the Fabric Structure

From the comparison of isolated failure end characteristics and accompanying fabric constraint, we can make the following observations: Abrupt yarn failure ends occur with high fabric constraint accompanied by short recovery length and with an indication of failure at yarn bends. Longer failure zones, *i.e.*, failure ends with long fiber tails, occur in the presence of low fabric constraint and long recovery length. Here the yarn behaves more like a long gauge length specimen tested out of fabric. It follows that two possible cases of yarn failure mechanism can be proposed.

CASE I

When the fabric density in the loaded direction is high enough to cause jamming of cross yarns, such as was the case in warp direction loading of the G fabrics, some extent of bending remains in the warp yarn up to break. The loaded yarn receives axial tension and unbending deformation. If the lateral pressure is sufficiently high to prevent local fiber slippage during tensioning and unbending, the total strain of a segment of fiber in a yarn of a loaded fabric can be divided into two components: one component due to the axial yarn strain and the other to the unbending of the yarn during crimp interchange. Local fiber strain can be estimated as [1]

$$\epsilon_f(\phi, \alpha, \rho_f, \rho_i) = \epsilon_y \cos^2(\alpha) + \epsilon_{f,\text{bend}}(\phi, \alpha, \rho_f) - \epsilon_{f,\text{bend}}(\phi, \alpha, \rho_i) \quad , \quad (8)$$

where $\epsilon_f(\phi, \alpha, \rho_f, \rho_i)$ = total local fiber strain due to changing yarn curvature, ϵ_y = yarn axial strain, α = local helix angle, ρ_i, ρ_f = radius of curvature before and after yarn unbending, and ϕ = fiber angle position in yarn section.

Figure 12 shows the estimated local fiber strain of a yarn with 0.15 axial strain as a function of the extent of unbending and the yarn twist multiple for the G fabric. As expected, the innerside of the bend (at $\phi = 0$) in a yarn with a smaller twist multiple leads to higher local fiber strains than would be the case for the outside of the bend and in a yarn with higher twist multiples.

CASE II

When the fabric density in the loading direction is not high enough to cause jamming of cross yarns (such as in the filling direction loading of G fabrics), negligible undulation is expected in the loaded yarn near its breaking stress. The loaded yarn in this case also receives axial tension and unbending deformation, but due to the small lateral pressure at the contact zone, local fiber segment slippage is allowed. Therefore, the total strain of a segment of fiber in a yarn of a loaded fabric comes primarily from axial yarn strain. The local lateral pressure on each fiber is still somewhat higher than for the free yarn out of fabric structure.

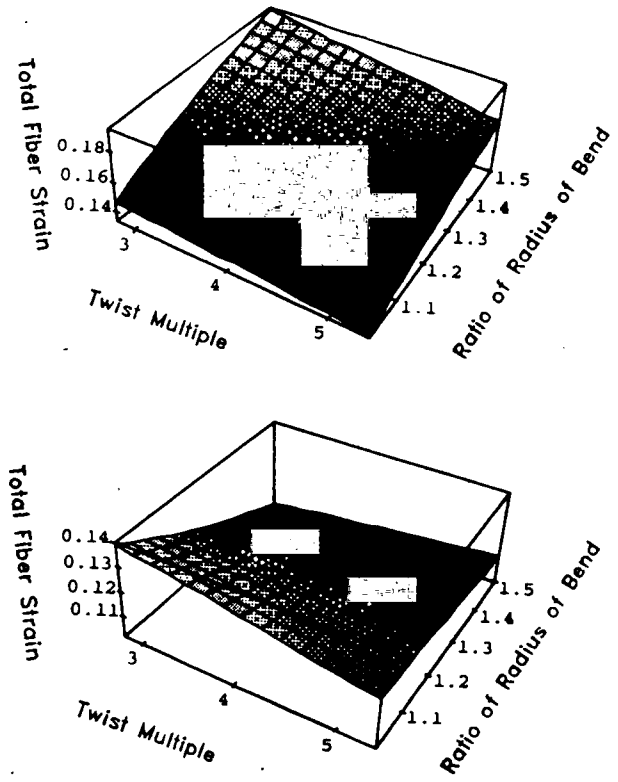

FIGURE 12. Local strain of a fiber at bent yarn surface with yarn axial strain 0.15 and no slippage condition. (top) total fiber strain at innerside of bend, (bottom) total fiber strain at outerside of bend.

Conclusions

From observations of yarn failure in uniaxially tensioned fabrics, we see that in tests of fabrics in a displacement controlled test, there are numerous isolated yarn failures, accompanied by significant tensile load drop at each failure. In many cases the magnitude of the load drop exceeded the average single yarn breaking strength.

Most of the isolated failures occurring in ring spun and rotor spun fabrics subjected to warpwise loading originated at bend locations. These yarns tended to break abruptly, with few protruding fiber ends, leading to a very short failure zone. This is very similar to the failure ends of yarns tested out of fabric at near zero gauge length. Similar observations were made for airjet spun fabrics loaded in the filling direction. Most isolated failures in ring spun fabrics tested fillingwise showed large amounts of long protruding fiber ends, leading to a very long failure zone. This is very similar to the failure ends of long gauge length yarns tested out of fabric.

The fiber ends of isolated yarn failures during warp loading evidence high lateral deformation, indicating the presence of high lateral pressures at yarn cross points. Some isolated warp yarn failure ends in ring spun fabrics exhibited multiple clusters of fiber breaks along the yarn, located at the inside of the crimp bends. We believe this to be a region of high tensile stress, as in the case for tensile straightening of a curved beam.

Isolated failures in different yarn systems showed different recovery lengths. Ring spun yarns showed longer recovery lengths than both rotor and airjet spun yarns of corresponding count and within the same fabric structure. Recovery length depended on fabric density. A dense fabric showed shorter recovery length than less dense fabric for the same yarn system.

From these results, we can conclude that the mechanism of yarn failure in a fabric subjected to uniaxial tensile testing is strongly influenced by fabric geometry at the *instant* of failure and by yarn properties both mechanical and topological. Further, when fabric density is high enough to create jamming of the cross yarn, yarn failure is initiated at the bending point where the highest local fiber strain will occur. In contrast, when fabric density is not high enough to cause jamming of the cross yarn, the yarn failure mechanism is comparable to yarn failure out of fabric, with some additional external lateral pressure.

ACKNOWLEDGMENTS

We would like to thank the Fibers Department of E. I. duPont de Nemours & Company, Inc., for providing financial and technical support of this work, and for the guidance and encouragement of staff members Dr. Don Shiffler and Dr. Frank Looney. Thanks are due as well to Springs Industries for providing yarns and fabrics for this study.

Literature Cited

1. Backer, S., Mechanics of Bent Yarns, *Textile Res. J.* **22**, 668 (1952).
2. Carnaby, G. A., and Grosberg, P., The Tensile Behavior of Staple yarns at Small Extensions, *J. Textile Inst.* **67**, 42 (1976).
3. Hearle, J. W. S., Grosberg, P., and Backer, S., "Structural Mechanics of Fibers, Yarns, and Fabrics," Wiley-Interscience, New York, 1969.
4. Lai, S. L., and Onions, W. J., The Lateral Crushing of Textile Fibers, *J. Textile Inst.* **64**, 175 (1973).
5. Lord, P. R., and Radhakrishnaiah, P., A Comparison of Various Woven Fabrics Containing Friction, Rotor, and Ring Spun Cotton Yarn Fillings, *Textile Res. J.* **58**, 354 (1988).
6. Lord, P. R., Radhakrishnaiah, P., and Grove, G., Assessment of the Tactile Properties of Woven Fabrics

Made from Various Types of Staple Fiber Yarn, *J. Textile Inst.* **79,** 32 (1988).

7. Machida, K., Masters thesis, Fibers and Polymers Division, M.I.T., Cambridge, MA, 1963.
8. Monego, C., and Backer, S., Tensile Rupture of Blended Yarns, *Textile Res. J.* **38,** 762 (1968).
9. Norota, S., Kawabata, S., and Kawai, H., Structure of Spun Yarn and Its Mechanical Non-Linear Property in the Initial Region of Tensile Deformation. Part I: Observation and Analysis of Spun Yarn, *Text. Mach. Soc. Jpn.* **16,** 41 (1970).
10. Realff, M. L., Seo, M., Boyce, M., Schwartz, P., and Backer, S. Mechanical Properties of Fabric Woven from Yarns Produced by Different Spinning Technologies, Yarn Failure as a Function of Gauge Length, *Textile Res. J.* **61,** 517 (1991).
11. Peirce, F. T., The Geometry of Cloth Structure, *J. Textile Inst.* **28,** T45 (1937).
12. Shahpurwala, A. A., and Schwartz, P., Modeling Woven Fabric Tensile Strength Using Statistical Bundle Theory, *Textile Res. J.* **59,** 26 (1989).
13. Tallant, J. D., Fiori, L. S., Little, H. W., and Castillon, A., Investigation of the Minimum Length of Cotton Fiber Effective in Single Yarn Tenacity, *Textile Res. J.* **34,** 1005 (1964).
14. Tallant, J. D., Shapiro, H. N., Sparer, G., Gaffney, H. E., and Armitage, R. H., Mathematical Aspects of Cotton Fiber Length Distribution under Various Breakage Models, *Textile Res. J.* **34,** 303 (1964).
15. Tallant, J. D., Pittman, R. A., and Schultz, E. F., Jr., The Changes in Fiber-Number Distribution under Various Breakage Models, *Textile Res. J.* **36,** 729 (1966).

Manuscript received May 15, 1992; accepted July 22, 1992.